Numer. Math. Theor. Meth. Appl.
doi: 10.4208/nmtma.2016.m1523

Vol. **9**, No. 3, pp. 470-496
August 2016

Finite Volume Element Methods for Two-Dimensional Three-Temperature Radiation Diffusion Equations

Yanni Gao[1], Xiukun Zhao[2], and Yonghai Li[1,*]

[1] *School of Mathematics, Jilin University, Changchun 130012, Jilin, People's Republic of China.*
[2] *Department of Mathematics and Computer Science, Eindhoven University of Technology, 5600MB Eindhoven, The Netherlands.*

Received 25 September 2015; Accepted 26 November 2015

Abstract. Two-dimensional three-temperature (2-D 3-T) radiation diffusion equations are widely used to approximately describe the evolution of radiation energy within a multi-material system and explain the exchange of energy among electrons, ions and photons. Their highly nonlinear, strong discontinuous and tightly coupled phenomena always make the numerical solution of such equations extremely challenging. In this paper, we construct two finite volume element schemes both satisfying the discrete conservation property. One of them can well preserve the positivity of analytical solutions, while the other one does not satisfy this property. To fix this defect, two as repair techniques are designed. In addition, as the numerical simulation of 2-D 3-T equations is very time consuming, we also devise a mesh adaptation algorithm to reduce the cost. Numerical results show that these new methods are practical and efficient in solving this kind of problems.

AMS subject classifications: 65N08, 65N12, 65N15

Key words: Two-dimensional three-temperature radiation diffusion equations; Finite volume element method; Energy conservation property; Repair technique; Mesh adaptation, Cutoff method.

1. Introduction

Radiation diffusion equations are widely used to simulate problems in inertial confinement fusion experiments, magnetic confinement fusion experiments, astrophysics problems, and so on. If radiation and material do not reach equilibrium, the equations are nonequilibrium radiation diffusion problems. 2-D 3-T radiation diffusion equations [12, 14–16, 25, 26] coupled with electron, ion and photon temperatures belong to nonequilibrium radiation diffusion problems. They are widely used to approximately describe the process of energy across multiple materials and the exchange of

*Corresponding author. *Email addresses:* yonghai@jlu.edu.cn (Y.-H. Li), gaoyn10@163.com (Y.-N. Gao), ying509501@126.com (X.-K. Zhao)

 ©2016 Global-Science Press

https://doi.org/10.4208/nmtma.2016.m1523 Published online by Cambridge University Press

energy among electrons, ions and photons. Because they have the characteristics of high nonlinearity, strong discontinuity and tight coupling, the numerical simulation of such equations is very challenging and interesting, which has attracted many authors' attention.

There are two key requirements desired to be satisfied in the numerical simulation of such problems. One is energy conservation property, the other is monotonicity, i.e. preserving positivity of analytical solutions. It is well known that the analytical solutions of the governing equations can satisfy some conservation forms inherently, but the numerical solutions can just satisfy the discrete analogue of these conservation forms [11, 13, 30]. So usually a discrete scheme is conservative, it means that this scheme can be expressed as the conservation form in a discrete sense. However, the numerical solutions of a conservative scheme are still very likely to appear negative solutions, which are not true because of the physics of the problem and will lead to the breakdown of computations. In order to deal with this problem, it is better to construct a discrete scheme which is unconditional monotone or monotone under less restrictive conditions [17, 18, 29, 32, 34, 39]. Monotone schemes are tightly connected to algebraic properties of the matrix of the discrete operator, and need impose severe restrictions on both meshes and problem coefficients. Therefore, the construction of monotone schemes is usually very difficult. Besides, some post-processing techniques such as the repair paradigms proposed in [19, 23, 31, 36] and the cutoff method analyzed in [24] can also be adapted to repair the negative solutions. The work mentioned above only focus on elliptic equations, diffusion problems with simple diffusion tensors and nonequilibrium radiation diffusion equations coupled with electron and ion temperatures. Next, we will introduce the existing work for 2-D 3-T radiation diffusion equations.

As to 2-D 3-T radiation diffusion equations, the relevant advances about numerical solutions can refer to [15, 26–28, 38]. In the framework of UG, the paper [26] successfully solved the problems by using the fully implicit finite volume scheme and parallel adaptive multigrid method on the triangular grids. The author discussed the influence of the particular time step chosen to computational efficiency detailedly. In the context of the symmetric finite volume scheme established in [27], two kinds of linearization methods, namely, Newton and "fixed-coefficient", have been researched in [28]. [15] constructed a symmetric finite volume element scheme which made the corresponding preconditioning technique applicable for 2-D 3-T radiation diffusion equations, and proposed a mesh adaptation approach based on monitor matrix. By this mesh adaptation, the energy conservation error and computation efficiency can be improved obviously. Through decoupling one temperature variable from the other two ones by a special coarsening strategy, [38] designed a two-level iterative method for solving the linear system discretized from 2-D 3-T radiation diffusion equations.

Finite volume element (FVE) methods are also called the generalized difference methods in China, belonging to the box schemes, or the control volume methods. Similar to the standard finite volume methods, we need to primarily integrate the governing equation on the control volume. Then, by using a finite element space to approximate

https://doi.org/10.4208/nmtma.2016.m1523 Published online by Cambridge University Press

the exact solutions, we obtain the corresponding finite volume element scheme. We refer readers to [2, 5, 6, 22, 45–50] for some recent advances on FVE methods. The linear element FVE method on triangular mesh for solving the standard linear second-order elliptic equation is studied in [10, 20, 21]. And the error estimates about this method are also discussed in these papers. In this paper, we extend the linear element FVE methods on triangular mesh to 2-D 3-T radiation diffusion equations. The nonlinearity and the discontinuity of the coupled equations bring difficulties to the numerical discretization. From the energy conservative form of the original system, we adopt some reasonable numerical integral formulas and approximate methods to deal with nonlinear terms and discontinuous coefficients. By various numerical integral formulas, we construct two kinds of conservative FVE schemes. The first one is very similar to the SFVEM constructed in [15] and seems to have better energy conservation property slightly. Here, we discuss its monotonicity in detail, which has never been done before. From the analysis of monotonicity and the numerical experiments, we know that the first one is monotone on many kinds of meshes, and the corresponding restrictive conditions of meshes are derived. However, the other one is nearly impossible to monotone and a large part of the numerical solutions would be negative at the start of actual calculation. Therefore, this scheme is usually considered not available. But we specially design two repair techniques for 2-D 3-T radiation diffusion equations, including the global repair technique and cutoff method, to overcome this defect. From the numerical results, we find that both of them could achieve good computational efficiency. And the cutoff method which has been known in [24] seems more preferred. Additionally, a spacial mesh adaptation algorithm based on the residual-type posteriori error estimator of FVE method is also proposed, by which the cost can be reduced observably.

The present paper is built up as follows. We describe the 2-D 3-T radiation diffusion equations briefly in Section 2. We derive two FVE schemes and analyze their energy conservation property and monotonicity in Section 3. Because the second scheme is hard to satisfy the monotonicity, repair techniques are extended to make this scheme preserve positivity in Section 4. In Section 5, we introduce a mesh adaptation algorithm. And then some numerical results are presented to highlight the correctness and efficiency of our methods in Section 6. Finally, some conclusions are given in Section 7.

2. 2-D 3-T radiation diffusion equations

The system of 3-T radiation diffusion equations is solved in a bounded open region Ω over the time interval $(0, \tau]$. As shown in Fig. 1, $\Omega = \bigcup_{k=1}^{3} \Omega_k$ is a half upper circle with radius $\mathcal{R}$ under two dimensional Cartesian coordinate system, and the circle center overlaps with the coordinate origin, diameter aligns with the x coordinate axis. In Ω, three different types of materials are included, where deuterium gas (DT) is filled in the innermost subdomain Ω_1 covering the area with $0 < r < \mathcal{R}_1$, glass (SiO2) is filled in the middle subdomain Ω_2 covering the area with $\mathcal{R}_1 < r < \mathcal{R}_2$, plastic foam (CH) is filled in the outside subdomain Ω_3. Γ_1 denotes the free boundary and Γ_2 denotes the

https://doi.org/10.4208/nmtma.2016.m1523 Published online by Cambridge University Press

symmetric boundary. Let $T = (T_e, T_i, T_r)$, then 2-D 3-T radiation diffusion equations coupled with electron temperature T_e, ion temperature T_i and photon temperature T_r are defined by

$$\begin{cases} \rho c_e \dfrac{\partial T_e}{\partial t} - \nabla \cdot (F_e) = S_e(T), & \text{(2.1a)} \\ \rho c_i \dfrac{\partial T_i}{\partial t} - \nabla \cdot (F_i) = S_i(T), & \text{in } \Omega \times (0, \tau] \quad \text{(2.1b)} \\ 4c_r T_r^3 \dfrac{\partial T_r}{\partial t} - \nabla \cdot (F_r) = S_r(T). & \text{(2.1c)} \end{cases}$$

For each unknown T_α, the corresponding flux vector F_α is defined by

$$F_\alpha = \kappa_\alpha \nabla T_\alpha,$$

where $\kappa_\alpha = A_\alpha T_\alpha^{5/2} (\alpha = e, i), \kappa_r = A_r T_r^{3+\sigma}$ are conductive coefficients of electron, ion and photon.

For $\alpha = e, i, r$, $S_\alpha(T)$ are the source terms, specifically formulated as

$$\begin{cases} S_e(T) = \rho\omega_{ei}(T_i - T_e) + \rho\omega_{er}(T_r - T_e), \\ S_i(T) = \rho\omega_{ei}(T_e - T_i), \\ S_r(T) = \rho\omega_{er}(T_e - T_r), \end{cases}$$

where $\omega_{ei} = \rho A_{ei} T_e^{-2/3}$ is the energy exchange coefficient between electron and ion, and $\omega_{er} = \rho A_{er} T_e^{-1/2}$ is the energy exchange coefficient between electron and photon.

According to physical experiments, the initial conditions are given by

$$T_\alpha(X, 0) = 3.0 \times 10^{-4}, \ X \in \Omega, \ \alpha = e, i, r.$$

The boundary conditions are defined as

- Symmetric: $\kappa_\alpha \frac{\partial T_\alpha}{\partial \mathbf{n}} \mid_{\Gamma_2} = 0, \alpha = e, i, r$, where $\mathbf{n}$ is the unit outer normal vector along boundary;
- Free: $\kappa_\alpha \frac{\partial T_\alpha}{\partial \mathbf{n}} \mid_{\Gamma_1} = 0, \alpha = e, i$; $T_r \mid_{\Gamma_1} = 2.0$.

Here ρ denotes the density of the medium. All parameters appeared in above description $\rho, c_\alpha, A_\alpha (\alpha = e, i, r), \sigma, A_{ei}, A_{er}$ are constants within each subdomain, but they are discontinuous across interfaces of subdomains. Mention that the values of the parameters will be given in Section 6.

In addition, the system energy of unit mass is defined by

$$\mathcal{E} = \mathcal{E}_e + \mathcal{E}_i + \mathcal{E}_r, \quad \mathcal{E}_e = c_e T_e, \quad \mathcal{E}_i = c_i T_i, \quad \mathcal{E}_r = \frac{1}{\rho} c_r T_r^4. \tag{2.2}$$

https://doi.org/10.4208/nmtma.2016.m1523 Published online by Cambridge University Press

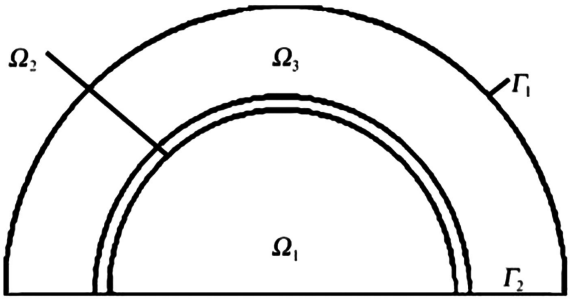


Figure 1: Computational domain Ω.

3. Finite volume element schemes

FVE methods are also called the generalized difference methods, the box schemes, or the control volume methods. Because FVE methods offer the flexibility to handle complicated geometries and follow the physical conservation law, including mass, momentum and energy, moreover are easy to be understood and implemented, FVE methods have been used widely in sciences and engineering, such as computational fluid mechanics, electromagnetics, petroleum reservoir simulations and other practical problems. The numerical analysis and general presentations of these methods are discussed concretely in [10, 20]. Let $0 = t_0 < t_1 < \cdots < t_{N-1} < t_N = \tau$. Integrating Eqs. (2.1a)-(2.1c) on the interval $[t_n, t_{n+1}]$, we have

$$\rho c_e(T_e(t_{n+1}) - T_e(t_n)) - \int_{t_n}^{t_{n+1}} \nabla \cdot (F_e)dt - \int_{t_n}^{t_{n+1}} S_e(T)dt = 0, \tag{3.1}$$

$$\rho c_i(T_i(t_{n+1}) - T_i(t_n)) - \int_{t_n}^{t_{n+1}} \nabla \cdot (F_i)dt - \int_{t_n}^{t_{n+1}} S_i(T)dt = 0, \tag{3.2}$$

$$c_r(T_r^4(t_{n+1}) - T_r^4(t_n)) - \int_{t_n}^{t_{n+1}} \nabla \cdot (F_r)dt - \int_{t_n}^{t_{n+1}} S_r(T)dt = 0, \tag{3.3}$$

For the temporal discretization, we use the backward Euler method to ensure the property of absolute numerical stability. Then, we obtain the nonlinear PDEs as follows:

$$\rho c_e(T_e^{n+1} - T_e^n) - \nabla \cdot (F_e^{n+1})\triangle t - S_e^{n+1}\triangle t = 0, \tag{3.4}$$

$$\rho c_i(T_i^{n+1} - T_i^n) - \nabla \cdot (F_i^{n+1})\triangle t - S_i^{n+1}\triangle t = 0, \tag{3.5}$$

$$c_r\big((T_r^{n+1})^4 - (T_r^n)^4\big) - \nabla \cdot (F_r^{n+1})\triangle t - S_r^{n+1}\triangle t = 0. \tag{3.6}$$

https://doi.org/10.4208/nmtma.2016.m1523 Published online by Cambridge University Press

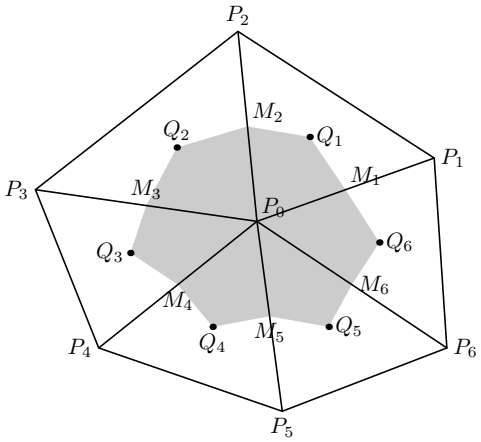


Figure 2: The dual element surrounding vertex P_0.

where $\triangle t = t^{n+1} - t^n$, T_α^n and T_α^{n+1} are temperature functions at times t^n and t^{n+1}, respectively, and $F_\alpha^{n+1}, S_\alpha^{n+1}$ are used to denote $F_\alpha(T^{n+1}), S_\alpha(T^{n+1})$ with $T^{n+1} = (T_e^{n+1}, T_i^{n+1}, T_r^{n+1})$.

We utilize the linear FVE method on triangular meshes to obtain spacial discretization. The specific construction procedure is as follows.

Let $\mathcal{T}_h$ be a triangular partition of computation domain Ω, which is called primary partition. For the triangulation $\mathcal{T}_h$, E_h denotes the set of edges and N_h is the set of vertices. The diameter of the triangular element $K \in \mathcal{T}_h$ and the length of the edge $l \in E_h$ are denoted by H_K and H_l, respectively.

We connect the barycenter point of every triangular element to its edge midpoints by straight line segments to obtain the dual partition. Fig. 2 shows that P_0 is an inner node, P_j $(j = 1, 2, \ldots, 6)$ are neighboring nodes around P_0, Q_j $(j = 1, 2, \ldots, 6)$ are barycenter points of triangular elements, and M_j $(j = 1, 2, \ldots, 6)$ are edge midpoints of primary elements. Connect M_j and Q_j $(j = 1, 2, \ldots, 6)$ successively to form a polygonal region $K_{P_0}^*$ surrounding P_0, called a dual element. The set of all the dual elements is denoted by $\mathcal{T}_h^*$, called the dual partition. Let S_Q and S_P^* denote the areas of the element K_Q and the dual element K_P^*, respectively.

Remark 3.1. In order to facilitate the application of FVE method, we assume that there is no mixed material element in the primary partition $\mathcal{T}_h$. In this case, some nodes of $\mathcal{T}_h$ appear on the interfaces of different material areas. Let Γ_{int} denote the interfaces of different material areas.

Define two finite dimensional trial function spaces associated with $\mathcal{T}_h$ by

$$U_h = \Big\{ u_h \in C(\overline{\Omega}) : u_h \mid_K \in \mathcal{P}^1, \quad \forall\, K \in \mathcal{T}_h \Big\}, \tag{3.7}$$

$$U_h^r = \Big\{ u_h \in C(\overline{\Omega}) : u_h \mid_K \in \mathcal{P}^1, \quad \forall\, K \in \mathcal{T}_h \ \text{ and } \ u_h \mid_{\Gamma_1} = 2.0 \Big\}, \tag{3.8}$$

where $\mathcal{P}^1$ consists of all the polynomials with a degree less than or equal to 1.

https://doi.org/10.4208/nmtma.2016.m1523 Published online by Cambridge University Press

Here, we introduce a linear transformation on triangle element K_Q,

$$\begin{cases} x = x_1\lambda_1 + x_2\lambda_2 + x_3\lambda_3, \\ y = y_1\lambda_1 + y_2\lambda_2 + y_3\lambda_3, \end{cases} \tag{3.9}$$

where

$$\lambda_1 = \frac{1}{2S_Q}\begin{vmatrix} x & y & 1 \\ x_2 & y_2 & 1 \\ x_3 & y_3 & 1 \end{vmatrix}, \quad \lambda_2 = \frac{1}{2S_Q}\begin{vmatrix} x_1 & y_1 & 1 \\ x & y & 1 \\ x_3 & y_3 & 1 \end{vmatrix}, \tag{3.10}$$

$$\lambda_3 = \frac{1}{2S_Q}\begin{vmatrix} x_1 & y_1 & 1 \\ x_2 & y_2 & 1 \\ x & y & 1 \end{vmatrix}, \quad S_Q = \frac{1}{2}\begin{vmatrix} x_1 & y_1 & 1 \\ x_2 & y_2 & 1 \\ x_3 & y_3 & 1 \end{vmatrix}, \tag{3.11}$$

and (x_i, y_i) is the coordinate of the vertex $P_i, i = 1, 2, 3$.

For any $u_h \in U_h$ or $u_h \in U_h^r$, set $u_i = u_h(P_i)$ $(i = 1, 2, 3)$ and then on the element K_Q, $u_h = u_1\lambda_1 + u_2\lambda_2 + u_3\lambda_3$.

Define the test function space associated with $\mathcal{T}_h^*$ by

$$V_h = \Big\{ v_h \in L^2(\Omega) : v_h \mid_{K_P^*} = \text{constant}, \ \ \forall\, P \in N_h \Big\}, \tag{3.12}$$

with the following basis functions (characteristic functions): for each $P \in N_h$,

$$\psi_P(X) = \begin{cases} 1, & \text{if } \ X \in K_P^*, \\ 0, & \text{if } \ X \notin K_P^*. \end{cases} \tag{3.13}$$

Multiply (3.4)-(3.6) by $\psi_P \in V_h$, integrate them on Ω, and use the Green's formula to obtain the following variational FVE form for (3.4)-(3.6): Find $T_{e,h}^{n+1}, T_{i,h}^{n+1} \in U_h, T_{r,h}^{n+1} \in U_h^r$, such that

$$\big(\rho c_e(T_{e,h}^{n+1} - T_{e,h}^n), \psi_P\big) + a_e(T_{e,h}^{n+1}, \psi_P)\triangle t - \big(S_{e,h}^{n+1}, \psi_P\big)\triangle t = 0, \tag{3.14}$$

$$\big(\rho c_i(T_{i,h}^{n+1} - T_{i,h}^n), \psi_P\big) + a_i(T_{i,h}^{n+1}, \psi_P)\triangle t - \big(S_{i,h}^{n+1}, \psi_P\big)\triangle t = 0, \tag{3.15}$$

$$\big(c_r((T_{r,h}^{n+1})^4 - (T_{r,h}^n)^4), \psi_P\big) + a_r(T_{r,h}^{n+1}, \psi_P)\triangle t - \big(S_{r,h}^{n+1}, \psi_P\big)\triangle t = 0, \tag{3.16}$$

where

$$a_\alpha(T_{\alpha,h}^{n+1}, \psi_P) = -\int_{\partial K_P^*} \kappa_{\alpha,h}^{n+1} \frac{\partial T_{\alpha,h}^{n+1}}{\partial \mathbf{n}} ds, \tag{3.17}$$

and $(\cdot, \cdot)$ is the standard inner product of the space $L^2(\Omega)$.

Based on various kinds of numerical methods, we construct two discrete schemes for 2-D 3-T radiation diffusion equations in the next installment.

https://doi.org/10.4208/nmtma.2016.m1523 Published online by Cambridge University Press

3.1. Scheme I

Because the parameters $\rho, c_e, c_i, c_r, A_e, A_i, A_r, \sigma, A_{ei}, A_{er}$ are discontinuous on the interfaces of different material areas, the approximate values of the parameters at these nodes located on the interfaces Γ_{int} need to be considered specially.

Let ε stand for some parameter. When the node P is not located on Γ_{int}, the value of ε at P is $\varepsilon(P)$. When the node P is located on Γ_{int}, the value of ε at P is approximated by the linear weighted combination of $\varepsilon(Q_j)$ $(j = 1, \ldots, N_P)$, namely

$$\varepsilon(P) := \sum_{j=1}^{N_P} \varepsilon(Q_j) \cdot \frac{S_{K_{Q_j} \cap K_P^*}}{S_P^*},$$

where Q_j are around P as shown in Fig. 2, and N_P denotes the number of elements around P throughout the paper. Actually, if P is not located on Γ_{int}, $\varepsilon(P) \equiv \varepsilon(Q_j)$ $(j = 1, \ldots, N_P)$ since ε is a constant in each subdomain.

We utilize a simple numerical integral formula, that is using the nodal value to replace the integrand, to obtain the approximations of integrals in (3.14)-(3.16):

$$\begin{aligned}
\big(\rho c_e(T_{e,h}^{n+1} - T_{e,h}^n), \psi_P\big) &= \int_{K_P^*} \rho c_e(T_{e,h}^{n+1} - T_{e,h}^n) dX \\
&:= \rho(P) c_e(P)(T_{e,h}^{n+1}(P) - T_{e,h}^n(P)) \cdot S_P^*, \qquad (3.18) \\
\big(\rho c_i(T_{i,h}^{n+1} - T_{i,h}^n), \psi_P\big) &= \int_{K_P^*} \rho c_i(T_{i,h}^{n+1} - T_{i,h}^n) dX \\
&:= \rho(P) c_i(P)(T_{i,h}^{n+1}(P) - T_{i,h}^n(P)) \cdot S_P^*, \qquad (3.19) \\
\big(c_r((T_{r,h}^{n+1})^4 - (T_{r,h}^n)^4), \psi_P\big) &= \int_{K_P^*} c_r((T_{r,h}^{n+1})^4 - (T_{r,h}^n)^4) dX \\
&:= c_r(P)((T_{r,h}^{n+1})^4(P) - (T_{r,h}^n)^4(P)) \cdot S_P^*, \qquad (3.20) \\
\big(S_{\alpha,h}^{n+1}, \psi_P\big) &= \int_{K_P^*} S_{\alpha,h}^{n+1} dX \\
&:= S_\alpha(T_h^{n+1}(P)) \cdot S_P^* (\alpha = e, i, r), \qquad (3.21)
\end{aligned}$$

where $T_h^{n+1}(P) = (T_{e,h}^{n+1}(P), T_{i,h}^{n+1}(P), T_{r,h}^{n+1}(P))$.

As shown in Fig. 2, the line integral along ∂K_P^* in (3.17) can be written as a summation of the integrals along the broken segments $\partial K_P^* \cap K_{Q_j} (j = 1, ..., N_P)$. Then using $\kappa_{\alpha,h}^{n+1}(Q_j)$ to approximate $\kappa_{\alpha,h}^{n+1}$ in the line integral, we have

$$a_\alpha(T_{\alpha,h}^{n+1}, \psi_P) := -\sum_{j=1}^{N_P} \kappa_{\alpha,h}^{n+1}(Q_j) \int_{\partial K_P^* \cap K_{Q_j}} \frac{\partial T_{\alpha,h}^{n+1}}{\partial \mathbf{n}} ds. \qquad (3.22)$$

https://doi.org/10.4208/nmtma.2016.m1523 Published online by Cambridge University Press

The aforementioned approximation, together with (3.18)-(3.22), yields

$$\rho(P)c_e(P)S_P^*\cdot T_{e,h}^{n+1}(P)-\triangle t\sum_{j=1}^{N_P}\kappa_{e,h}^{n+1}(Q_j)\int_{\partial K_P^*\cap K_{Q_j}}\frac{\partial T_{e,h}^{n+1}}{\partial \mathbf{n}}ds$$

$$-\triangle tS_e(T_h^{n+1}(P))\cdot S_P^*=\rho(P)c_e(P)S_P^*\cdot T_{e,h}^n(P), \tag{3.23}$$

$$\rho(P)c_i(P)S_P^*\cdot T_{i,h}^{n+1}(P)-\triangle t\sum_{j=1}^{N_P}\kappa_{i,h}^{n+1}(Q_j)\int_{\partial K_P^*\cap K_{Q_j}}\frac{\partial T_{i,h}^{n+1}}{\partial \mathbf{n}}ds$$

$$-\triangle tS_i(T_h^{n+1}(P))\cdot S_P^*=\rho(P)c_i(P)S_P^*\cdot T_{i,h}^n(P), \tag{3.24}$$

$$c_r(P)S_P^*\cdot(T_{r,h}^{n+1}(P))^4-\triangle t\sum_{j=1}^{N_P}\kappa_{r,h}^{n+1}(Q_j)\int_{\partial K_P^*\cap K_{Q_j}}\frac{\partial T_{r,h}^{n+1}}{\partial \mathbf{n}}ds$$

$$-\triangle tS_r(T_h^{n+1}(P))\cdot S_P^*=c_r(P)S_P^*\cdot(T_{r,h}^n(P))^4. \tag{3.25}$$

On any triangular element K_Q,

$$\frac{\partial u_h}{\partial x}=\frac{(y_2-y_3)\cdot u_1+(y_3-y_1)\cdot u_2+(y_1-y_2)\cdot u_3}{2S_Q}, \tag{3.26}$$

$$\frac{\partial u_h}{\partial y}=\frac{(x_3-x_2)\cdot u_1+(x_1-x_3)\cdot u_2+(x_2-x_1)\cdot u_3}{2S_Q}, \tag{3.27}$$

where $(x_j,y_j)(j=1,2,3)$ are the coordinates of three vertexes on K_Q, $u_j=u_h(x_j,y_j)$ $(j=1,2,3)$.

Then, by a simple calculation, it follows that

$$\int_{\partial K_P^*\cap K_{Q_j}}\frac{\partial T_{\alpha,h}^{n+1}}{\partial \mathbf{n}}ds=\int_{\partial K_P^*\cap K_{Q_j}}\left(\frac{\partial T_{\alpha,h}^{n+1}}{\partial x}dy-\frac{\partial T_{\alpha,h}^{n+1}}{\partial y}dx\right)$$

$$=-\frac{|\overrightarrow{P_jP_{j+1}}|^2}{4S_{Q_j}}T_{\alpha,h}^{n+1}(P)+\frac{\overrightarrow{PP_{j+1}}\cdot\overrightarrow{P_jP_{j+1}}}{4S_{Q_j}}T_{\alpha,h}^{n+1}(P_j) \tag{3.28}$$

$$+\frac{\overrightarrow{P_jP}\cdot\overrightarrow{P_jP_{j+1}}}{4S_{Q_j}}T_{\alpha,h}^{n+1}(P_{j+1}),$$

where $N_P+1=1$. Substituting (3.28) into (3.23)-(3.25), we gain the fully discrete scheme of (3.14)-(3.16) on any triangular partition.

3.2. Scheme II

We compute the integrals of (3.14)-(3.16) by another method, and the discretizations of line integrals in (3.17) are the same as Scheme I. For the other integrals in

https://doi.org/10.4208/nmtma.2016.m1523 Published online by Cambridge University Press

(3.14)-(3.16), we employ the following way to approximate. Because the three Eqs. (3.14)-(3.16) have the same form, we just give the discretization of Eq. (3.16) in detail. Firstly, the first term on the left side of Eq. (3.16) is approximated by

$$\begin{aligned}
&\Big(c_r((T_{r,h}^{n+1})^4-(T_{r,h}^{n})^4),\psi_P\Big)\\
&=\int_{K_P^*}c_r((T_{r,h}^{n+1})^4-(T_{r,h}^{n})^4)dX=\sum_{j=1}^{N_P}\int_{K_P^*\cap K_{Q_j}}c_r((T_{r,h}^{n+1})^4-(T_{r,h}^{n})^4)dX\\
&:=\sum_{j=1}^{N_P}c_r(Q_j)\bigg((T_{r,h}^{n+1}(P))^3\int_{K_P^*\cap K_{Q_j}}T_{r,h}^{n+1}dX-(T_{r,h}^{n}(P))^3\int_{K_P^*\cap K_{Q_j}}T_{r,h}^{n}dX\bigg). \qquad (3.29)
\end{aligned}$$

Secondly, we discrete the source term in Eq. (3.16) as

$$\begin{aligned}
&\big(S_{r,h}^{n+1},\psi_P\big)=\int_{K_P^*}\rho^2A_{er}(T_{e,h}^{n+1})^{-1/2}(T_{e,h}^{n+1}-T_{r,h}^{n+1})dX\\
&=\sum_{j=1}^{N_P}\int_{K_P^*\cap K_{Q_j}}\rho^2A_{er}(T_{e,h}^{n+1})^{-1/2}(T_{e,h}^{n+1}-T_{r,h}^{n+1})dX\\
&:=\sum_{j=1}^{N_P}\rho^2(Q_j)A_{er}(Q_j)(T_{e,h}^{n+1}(P))^{-1/2}\int_{K_P^*\cap K_{Q_j}}(T_{e,h}^{n+1}-T_{r,h}^{n+1})dX. \qquad (3.30)
\end{aligned}$$

By exactly integrating the aforementioned equations (3.29) and (3.30), we establish another discrete scheme for the 2-D 3-T radiation diffusion equations.

3.3. Energy conservation and monotonicity

We already present two different numerical schemes for solving 2-D 3-T radiation diffusion equations, and then, we will compare them by theoretical analysis and numerical tests.

Firstly, we analysis their energy conservation property by the concepts of differential and discrete conservation [11, 13, 30]. The conservation property of the governing equations (2.1a)-(2.1c) can be illustrated by integrating them over domain $\Omega\times[0,\tau]$, and applying Green's formula to the divergence yields

$$\int_\Omega\rho c_eT_e(X,\tau)dX-\int_\Omega\rho c_eT_e(X,0)dX-\int_0^\tau dt\int_\Omega S_e(T)dX=0, \qquad (3.31)$$

$$\int_\Omega\rho c_iT_i(X,\tau)dX-\int_\Omega\rho c_iT_i(X,0)dX-\int_0^\tau dt\int_\Omega S_i(T)dX=0, \qquad (3.32)$$

$$\int_\Omega c_rT_r^4(X,\tau)dX-\int_\Omega c_rT_r^4(X,0)dX-\int_0^\tau dt\int_\Omega S_r(T)dX$$

https://doi.org/10.4208/nmtma.2016.m1523 Published online by Cambridge University Press

$$-\int_0^\tau dt \int_{\Gamma_1} F_r \cdot \mathbf{n} ds = 0. \tag{3.33}$$

From the definition (2.2), we know that Eqs. (3.31)-(3.33) can be seen as a statement of global energy conservation equation. Taking the sum of (3.31)-(3.33), we obtain another simplified form

$$\sum_{\alpha=e,i} \left(\int_\Omega \rho c_\alpha T_\alpha(X,\tau) dX - \int_\Omega \rho c_\alpha T_\alpha(X,0) dX \right) + \int_\Omega c_r T_r^4(X,\tau) dX - \int_\Omega c_r T_r^4(X,0) dX - \int_0^\tau dt \int_{\Gamma_1} F_r \cdot \mathbf{n} ds = 0. \tag{3.34}$$

For numerical solutions, they can not satisfy exactly the analytic statements of conservative equations (3.31)-(3.33) and (3.34). Usually, we call a discrete numerical scheme is conservative, if the discrete integral of a certain quantity is preserved by this scheme. In Scheme I (3.23)-(3.25), summing the discrete equations over node P and time level n, respectively, we have

$$\sum_{P\in N_h} (\rho c_e T_{e,h}^N)(P) \cdot S_P^* - \sum_{P\in N_h} (\rho c_e T_{e,h}^0)(P) \cdot S_P^* - \sum_{n=1}^N \left(\sum_{P\in N_h} S_e(T_h^n(P)) \cdot S_P^* \right) \triangle t = 0, \tag{3.35}$$

$$\sum_{P\in N_h} (\rho c_i T_{i,h}^N)(P) \cdot S_P^* - \sum_{P\in N_h} (\rho c_i T_{i,h}^0)(P) \cdot S_P^* - \sum_{n=1}^N \left(\sum_{P\in N_h} S_i(T_h^n(P)) \cdot S_P^* \right) \triangle t = 0, \tag{3.36}$$

$$\sum_{P\in N_h} (c_r (T_{e,h}^N)^4)(P) \cdot S_P^* - \sum_{P\in N_h} (c_r (T_{e,h}^0)^4)(P) \cdot S_P^* - \sum_{n=1}^N \left(\sum_{P\in N_h} S_r(T_h^n(P)) \cdot S_P^* \right) \triangle t - \sum_{n=1}^N \left(\sum_{P\in N_h^1} \int_{\partial K_P^* \cap \Gamma_1} F_{r,h}^n \cdot \mathbf{n} ds \right) \triangle t = 0, \tag{3.37}$$

where $T_h^n(P) = (T_{e,h}^n(P), T_{i,h}^n(P), T_{r,h}^n(P))$ and N_h^1 denotes the set of nodes located on the boundary Γ_1. Further more, by the definition of S_α and taking the summation of Eqs. (3.35)-(3.37), it follows that

$$\sum_{P\in N_h} (\rho c_e T_{e,h}^N)(P) \cdot S_P^* - \sum_{P\in N_h} (\rho c_e T_{e,h}^0)(P) \cdot S_P^* + \sum_{P\in N_h} (\rho c_i T_{i,h}^N)(P) \cdot S_P^* - \sum_{P\in N_h} (\rho c_i T_{i,h}^0)(P) \cdot S_P^* + \sum_{P\in N_h} (c_r (T_{e,h}^N)^4)(P) \cdot S_P^* - \sum_{P\in N_h} (c_r (T_{e,h}^0)^4)(P) \cdot S_P^* - \sum_{n=1}^N \left(\sum_{P\in N_h^1} \int_{\partial K_P^* \cap \Gamma_1} F_{r,h}^n \cdot \mathbf{n} ds \right) \triangle t = 0. \tag{3.38}$$

It can be observed that Eqs. (3.35)-(3.37) and (3.38) are the discrete analogues of equations (3.31)-(3.33) and (3.34), respectively. Therefore, Scheme I satisfies the total energy conservation in a discrete sense. As to Scheme II, the computation of line

https://doi.org/10.4208/nmtma.2016.m1523 Published online by Cambridge University Press

integrals is the same as that in Scheme I, just the approximation of double integrals on dual elements is different. Using analogical analysis as Scheme I, we can get another discrete analogue of equations (3.31)-(3.33) and (3.34). The discrete equations corresponding to Scheme II can be expressed in the form of (3.35)-(3.37) and (3.38). So they both discretely conserve the vector $T = (T_e, T_i, T_r)$ in space and time.

Next, we discuss the monotonicity of these two discrete schemes. The monotonicity of discrete solutions is an interesting topic, which has attracted the attention of many scholars [17,18,29,32,39]. And so far, the M-matrix is still the most universal standard in terms of the monotonicity.

Let $U^n = (T^n_{e,1}, T^n_{i,1}, T^n_{r,1}, T^n_{e,2}, T^n_{i,2}, T^n_{r,2}, \cdots, T^n_{e,\mathfrak{J}}, T^n_{i,\mathfrak{J}}, T^n_{r,\mathfrak{J}})$, where $T^n_{e,m} = T^n_{e,h}(P_m)$, $T^n_{i,m} = T^n_{i,h}(P_m), T^n_{r,m} = T^n_{r,h}(P_m)(m = 1, 2, \cdots, \mathfrak{J})$, and $\mathfrak{J}$ is the number of nodes of $\mathcal{T}_h$. Thus, discrete schemes in last subsection can be written as

$$A(U^{n+1})U^{n+1} = F(U^n). \tag{3.39}$$

The system (3.39) is nonlinear, which is caused by nonlinear equations (2.1a)-(2.1c), rather than by our discrete methods. In the beginning of discussing the monotonicity, we use the Picard iterations to linearize (3.39) [15]. Then, (3.39) can be written as a linear algebraic system

$$A(U^{(n)})U^{n+1} = F(U^n), \tag{3.40}$$

where $U^{(n)} = (T^{(n)}_{e,1}, T^{(n)}_{i,1}, T^{(n)}_{r,1}, T^{(n)}_{e,2}, T^{(n)}_{i,2}, T^{(n)}_{r,2}, \cdots, T^{(n)}_{e,\mathfrak{J}}, T^{(n)}_{i,\mathfrak{J}}, T^{(n)}_{r,\mathfrak{J}})$ is the latest solution functions of linear equations in the nonlinear iteration. Since a M-matrix [35] guarantees that the solution of a system of linear algebraic equations will be non-negative for any non-negative right hand side, the analysis of monotonicity is usually come down to analyze the algebraic properties of the matrix of the discrete operator.

For a general irreducible matrix A, A is a M-matrix when it satisfies the following three properties [1]:

1. All diagonal entries of matrix A are positive.

2. All off-diagonal entries of matrix A would be non-positive.

3. Every row sum in matrix A is nonnegative, and at least one of them is positive.

Let us recall Scheme I first. After computing the line integral exactly and linearizing,

https://doi.org/10.4208/nmtma.2016.m1523 Published online by Cambridge University Press

(3.25) becomes

$$\sum_{j=1}^{N_P}\Bigg(\Bigg(c_r(T_{r,h}^{(n)}(P))^3\frac{S_{Q_j}}{3}+\triangle t\rho^2 Aer(T_{e,h}^{(n)}(P))^{-2/3}\frac{S_{Q_j}}{3}+\triangle t\kappa_{r,h}^{(n)}(Q_j)\frac{|\overrightarrow{P_jP_{j+1}}|^2}{4S_{Q_j}}\Bigg)\cdot T_{r,h}^{n+1}(P)$$
$$-\triangle t\rho^2 Aer(T_{e,h}^{(n)}(P))^{-2/3}\frac{S_{Q_j}}{3}\cdot T_{e,h}^{n+1}(P)-\triangle t\kappa_{r,h}^{(n)}(Q_j)\Bigg(\frac{\overrightarrow{PP_{j+1}}\cdot\overrightarrow{P_jP_{j+1}}}{4S_{Q_j}}\Bigg)\cdot T_{r,h}^{n+1}(P_j)$$
$$-\triangle t\kappa_{r,h}^{(n)}(Q_j)\Bigg(\frac{\overrightarrow{P_jP}\cdot\overrightarrow{P_jP_{j+1}}}{4S_{Q_j}}\Bigg)\cdot T_{r,h}^{n+1}(P_{j+1})\Bigg)$$
$$=\sum_{j=1}^{N_P}c_r(Q_j)\frac{S_{Q_j}}{3}(T_{r,h}^{n}(P))^4, \tag{3.41}$$

where $N_P+1=1$. (3.23) and (3.24) have the similar expressions. It is obvious that the matrix $A(U^{(n)})$ satisfies property 1 for any vector $U^{(n)}\geq 0$. Because

$$\kappa_{r,h}^{(n)}(Q_j)\frac{|\overrightarrow{P_jP_{j+1}}|^2}{4S_{Q_j}}-\kappa_{r,h}^{(n)}(Q_j)\frac{\overrightarrow{PP_{j+1}}\cdot\overrightarrow{P_jP_{j+1}}}{4S_{Q_j}}-\kappa_{r,h}^{(n)}(Q_j)\frac{\overrightarrow{P_jP}\cdot\overrightarrow{P_jP_{j+1}}}{4S_{Q_j}}=0, \tag{3.42}$$

the row sum in matrix $A(U^{(n)})$ equal to $c_r(T_{r,h}^{(n)}(P))^3\frac{S_{Q_j}}{3}$, which is positive, i.e., the matrix $A(U^{(n)})$ satisfies property 3. Moreover, if $\overrightarrow{PP_{j+1}}\cdot\overrightarrow{P_jP_{j+1}}\geq 0$ and $\overrightarrow{P_jP}\cdot\overrightarrow{P_jP_{j+1}}\geq 0$, $A(U^{(n)})$ satisfies property 2. In conclusion, $A(U^{(n)})$ is a M-matrix for any vector $U^{(n)}\geq 0$ if and only if the maximal interior angle of the primary partition is not greater than 90°. Scheme I is monotone under this given condition. Next, we concentrate on Scheme II. The matrix $A(U^{(n)})$ still satisfies properties 1 and 3. However, the second property of the M-matrix is so hard to be achieved, because many positive terms are added to off-diagonal positions. For example, the coefficient before $T_{r,h}^{n+1}(P_j)$ becomes

$$c_r(T_{r,h}^{(n)}(P))^3\frac{7S_{Q_j}}{108}+\triangle t\rho^2 Aei(T_{e,h}^{(n)}(P))^{-\frac{2}{3}}\frac{7S_{Q_j}}{108}-\triangle t\kappa_{r,h}^{(n)}(Q_j)\frac{\overrightarrow{PP_{j+1}}\cdot\overrightarrow{P_jP_{j+1}}}{4S_{Q_j}}. \tag{3.43}$$

(3.43) is an off-diagonal value of $A(U^{(n)})$, so it should be nonpositive when $A(U^{(n)})$ satisfies property 2. In physical experiments, the value of $\rho^2 Aei(T_{e,h}^{(n)}(P))^{-2/3}$ is very large. If Scheme II is monotone, the constraint for meshes is quite harsh. This is hard to be realized in practice.

4. Repair techniques

Scheme II is not monotone based on the above analysis in Section 3. And in the numerical experiments underlying Scheme II, a large part of the numerical solution become negative at the beginning of computation. The negative solution is not true because of the physics of the problem, and leads to the breakdown of computation

https://doi.org/10.4208/nmtma.2016.m1523 Published online by Cambridge University Press

because both the energy exchange coefficients and diffusion coefficients include radical signs. In this paper, we employ two post-processing techniques to deal with the problem.

The first one is called global repair technique which can preserve the total energy conservation. It is proposed in [19, 36] to deal with elliptic problems. We extend it to 2-D 3-T radiation diffusion equations. Define the total energy

$$\mathcal{E}_{total} = \sum_{j=1}^{\mathfrak{J}} \Big(\rho c_e T_{e,h}(P_j) + \rho c_i T_{i,h}(P_j) + c_r (T_{r,h}(P_j))^4 \Big) S^*_{P_j}, \tag{4.1}$$

where $\mathfrak{J}$ is the number of nodes of $\mathcal{T}_h$. Let $T_{e,min} = \min T^0_e$, $T_{i,min} = \min T^0_i$, $T_{r,min} = \min T^0_r$, where T^0_e, T^0_i and T^0_r are obtained by the initial condition. Each negative value $T_{\alpha,h}(P_j)$ is replaced by the minimum $T_{\alpha,min} (\alpha = e, i, r)$. Let $T^u_{\alpha,h}$ denote the unrepaired solution, and $T^r_{\alpha,h}$ denote the repaired solution. The total energy of the unrepaired solution is

$$\mathcal{E}^u_{total} = \sum_{j=1}^{\mathfrak{J}} \Big(\rho c_e T^u_{e,h}(P_j) + \rho c_i T^u_{i,h}(P_j) + c_r (T^u_{r,h}(P_j))^4 \Big) S^*_{P_j}, \tag{4.2}$$

and we require that the modified solution has the same total energy, namely

$$\mathcal{E}^r_{total} = \sum_{j=1}^{\mathfrak{J}} \Big(\rho c_e T^r_{e,h}(P_j) + \rho c_i T^r_{i,h}(P_j) + c_r (T^r_{r,h}(P_j))^4 \Big) S^*_{P_j} = \mathcal{E}^u_{total}. \tag{4.3}$$

For $\alpha = e, i, r,$ we divide N_h into two classes:

$$J_{T_e,p} = \big\{ j_e; j_e \in N_h, T^u_{e,h}(j_e) \geq T_{e,min} \big\},$$
$$J_{T_i,p} = \big\{ j_i; j_i \in N_h, T^u_{i,h}(j_i) \geq T_{i,min} \big\},$$
$$J_{T_r,p} = \big\{ j_r; j_r \in N_h, T^u_{r,h}(j_r) \geq T_{r,min} \big\},$$

and

$$J_{T_e,n} = \big\{ j_e; j_e \in N_h, T^u_{e,h}(j_e) < T_{e,min} \big\},$$
$$J_{T_i,n} = \big\{ j_i; j_i \in N_h, T^u_{i,h}(j_i) < T_{i,min} \big\},$$
$$J_{T_r,n} = \big\{ j_r; j_r \in N_h, T^u_{r,h}(j_r) < T_{r,min} \big\}.$$

Define

$$\mathcal{E}_{T_e,p} = \sum_{j \in J_{T_e,p}} \rho c_e (T^u_{e,h}(j) - T_{e,min}) S^*_j,$$
$$\mathcal{E}_{T_i,p} = \sum_{j \in J_{T_i,p}} \rho c_i (T^u_{i,h}(j) - T_{i,min}) S^*_j,$$
$$\mathcal{E}_{T_r,p} = \sum_{j \in J_{T_i,p}} c_r ((T^u_{r,h}(j))^4 - (T_{r,min})^4) S^*_j,$$

https://doi.org/10.4208/nmtma.2016.m1523 Published online by Cambridge University Press

as the total energy, which is available in the whole region, and

$$\mathcal{E}_{T_e,n} = -\sum_{j\in J_{T_e,n}} \rho c_e (T^u_{e,h}(j) - T_{e,min}) S^*_j,$$
$$\mathcal{E}_{T_i,n} = -\sum_{j\in J_{T_i,n}} \rho c_i (T^u_{i,h}(j) - T_{i,min}) S^*_j,$$
$$\mathcal{E}_{T_r,n} = -\sum_{j\in J_{T_i,n}} c_r ((T^u_{r,h}(j))^4 - (T_{r,min})^4) S^*_j,$$

as the total energy, which is needed in the whole region. For 2-D 3-T radiation diffusion equations, the temperature $T_{r,h}$ is easy to be negative in the process of the computation, and the proportion of negative solutions in the whole solution vector is very large. In this case, the needed energy $\mathcal{E}_{T_r,n}$ will greater than the available energy $\mathcal{E}_{T_r,p}$. Therefore, it is not applicable to repair these three temperatures separately. In the following, we take them as a whole to repair the negative values. Define $\mathcal{E}_p = \mathcal{E}_{T_e,p} + \mathcal{E}_{T_i,p} + \mathcal{E}_{T_r,p}$ and $\mathcal{E}_n = \mathcal{E}_{T_e,n} + \mathcal{E}_{T_i,n} + \mathcal{E}_{T_r,n}$. Let

$$T^r_{\alpha,h}(j_\alpha) = T_{\alpha,min}, \quad \forall\ j_\alpha \in J_{T_\alpha,n}, \alpha = e,i,r. \tag{4.4}$$

Furthermore,

$$T^r_{\alpha,h}(j_\alpha) = T^u_{\alpha,h}(j_\alpha) - \frac{\mathcal{E}_{T_\alpha,j_\alpha}\frac{\mathcal{E}_n}{\mathcal{E}_p}}{\rho c_\alpha S^*_{j_\alpha}}, \quad \forall\ j_\alpha \in J_{T_\alpha,p}, \alpha = e,i, \tag{4.5}$$

$$T^r_{r,h}(j_r) = \left((T^u_{r,h}(j_r))^4 - \frac{\mathcal{E}_{T_r,j_r}\frac{\mathcal{E}_n}{\mathcal{E}_p}}{c_r S^*_{j_r}}\right)^{1/4}, \quad \forall\ j_r \in J_{T_r,p}, \tag{4.6}$$

where

$$\mathcal{E}_{T_\alpha,j_\alpha} = \rho c_\alpha (T^u_{\alpha,h}(j_\alpha) - T_{\alpha,min}) S^*_{j_\alpha},\ \ j_\alpha \in J_{T_\alpha,p},\ \alpha = e,i,$$
$$\mathcal{E}_{T_r,j_r} = c_r ((T^u_{r,h}(j_r))^4 - (T_{r,min})^4) S^*_{j_r},\ \ j_r \in J_{T_r,p}.$$

From (4.4)-(4.6), it follows that $\mathcal{E}^r_{total} = \mathcal{E}^u_{total}$. Thus, the global repair technique dose not change the total inner energy.

On the other hand, we can repair the numerical solutions by replacing the negative solution by a relevant value. The idea of this method comes from the cutoff method proposed and analyzed in [24]. We still use the notations defined above. And denote the numerical solutions at the former time level by $T^n_{\alpha,h}$, additionally. Let

$$T^r_{\alpha,h}(j_\alpha) = T^n_{\alpha,h}(j_\alpha), \quad \forall\ j_\alpha \in J_{T_\alpha,n}, \alpha = e,i,r, \tag{4.7}$$

$$T^r_{\alpha,h}(j_\alpha) = T^u_{\alpha,h}(j_\alpha), \quad \forall\ j_\alpha \in J_{T_\alpha,p}, \alpha = e,i,r. \tag{4.8}$$

Obviously, this method would change the total inner energy at every time level, but is applicable for 2-D 3-T radiation diffusion equations.

https://doi.org/10.4208/nmtma.2016.m1523 Published online by Cambridge University Press

5. Mesh adaptation

Posteriori error estimators are indispensable in adaptive computations. There are general three types of posteriori error estimators: residual type, recovery type and hierarchical type. We refer readers to [41, 45–48] and references therein for detailed research on recovery type and hierarchical type posteriori error estimations. In this paper, we employ the residual type estimator to conduct the adaptive computation. In [37], the authors proved the residual posteriori error estimate of the finite volume element method on triangular mesh for the general two dimensional nonlinear parabolic equation. Based on this theoretical result, we develop a adaptive algorithm for 2-D 3-T radiation diffusion equations. Here, we briefly describe the relevant theory.

Let $T_h = (T_{e,h}, T_{i,h}, T_{r,h})$ be the numerical solutions at some time level, $K_1 \in \mathcal{T}_h$ and $K_2 \in \mathcal{T}_h$ two adjacent elements, $l \in E_h$ the common edge of K_1 and K_2. If $l \in \partial\Omega$, l is supposed to be located on K_1. Then jumps $\mathcal{J}_l^\alpha(\alpha = e, i, r)$ across l are expressed as follows:

$$\mathcal{J}_l^\alpha = \begin{cases} \mathbf{n}_1 \cdot \left(\kappa_{\alpha,h} \nabla T_{\alpha,h}\right)_{K_1} + \mathbf{n}_2 \cdot \left(\kappa_{\alpha,h} \nabla T_{\alpha,h}\right)_{K_2}, & \text{if } l \in E_h \setminus \partial\Omega, \\ \mathbf{n}_1 \cdot \left(\kappa_{\alpha,h} \nabla T_{\alpha,h}\right)_{K_1}, & \text{if } l \in E_h \cap \partial\Omega, \end{cases} \tag{5.1}$$

where $\mathbf{n}_1$ is the unit normal vector to l pointing from K_1 to K_2 and $\mathbf{n}_2$ is the unit normal vector in contrast to $\mathbf{n}_1$. For any element $K \in \mathcal{T}_h$, we introduce the element residual $\mathcal{R}_K^\alpha(\alpha = e, i, r)$:

$$\mathcal{R}_K^\alpha = \left(\rho c_\alpha \frac{\partial T_{\alpha,h}}{\partial t} - \nabla \cdot (\kappa_{\alpha,h} \nabla T_{\alpha,h}) - S_\alpha(T_h)\right)_K, \quad \alpha = e, i, \tag{5.2}$$

$$\mathcal{R}_K^r = \left(4c_r (T_{r,h})^3 \frac{\partial T_{r,h}}{\partial t} - \nabla \cdot (\kappa_{r,h} \nabla T_{r,h}) - S_r(T_h)\right)_K. \tag{5.3}$$

Now, we give the main result for posterior error estimates.

Theorem 5.1. *Suppose that γ, θ are two positive constants, only associated with the smallest inner angle of the triangulation $\mathcal{T}_h$. Then it holds that*

$$\| \mathcal{R}_h \|_{H^*} = \sup_{0 \neq \varphi \in H^1(\Omega)} \frac{|< \mathcal{R}_h, \varphi >|}{\| \varphi \|_{H^1}} \leq C \left\{ \sum_{K \in \mathcal{T}_h} (\eta_K)^2 \right\}^{1/2}, \tag{5.4}$$

where

$$\eta_K = \sum_{\alpha = e,i,r} \gamma H_K \| \mathcal{R}_K^\alpha \|_{L^2} + \theta \left\{ \frac{1}{2} \sum_{l \in \partial K} H_l \| \mathcal{J}_l^\alpha \|_{L^2}^2 \right\}^{1/2}, \tag{5.5}$$

and H^* is the dual space of $H^1(\Omega)$, $\mathcal{R}_h$ is the total residual.

The proof of Theorem 5.1 is similar to that in [37]. We refer readers to [37] for more details.

According to the theory of mesh adaptation based on the posteriori error indicator η_K, we design the following algorithm for Eqs. (2.1a)-(2.1c).

https://doi.org/10.4208/nmtma.2016.m1523 Published online by Cambridge University Press

Algorithm 5.1. *Let $\mathcal{T}_0^h$ be the initial adaptive triangulation which can be generated by the initial conditions, and $\mathcal{T}_k^h(k = 0, 1, 2, \cdots)$ be the kth adaptive grid, then find the adaptive grid $\mathcal{T}_{k+1}^h$:*

(i) *Solve the nonlinear PDEs* (3.4)-(3.6) *with the finite volume element scheme constructed in Section 3 on mesh $\mathcal{T}_k^h$;*

(ii) *Calculate the posteriori error indicator η_K on each element of $\mathcal{T}_k^h$;*

(iii) *Mark the element K to refine, on which η_K is greater than a given value. And mark the element K to coarsen, on which η_K is very small;*

(iv) *Create adaptive grid $\mathcal{T}_{k+1}^h$ by refining and coarsening the marked elements of $\mathcal{T}_k^h$.*

6. Numerical Test

In this section, some numerical results are presented to indicate how our schemes and post-processing techniques work in terms of preserving positivity and maintaining energy conservation. A comparison between our schemes and another numerical scheme proposed in [15] can be seen directly. Besides, the numerical efficiency of mesh adaptation is also presented.

We take the typical model of laser-driven implosion of inertial confinement fusion in paper [26] as a benchmark. Deuterium gas (DT), glass (SiO2) and plastic foam (CH) are filled into subdomain $\Omega_1, \Omega_2, \Omega_3$ respectively. Below are the values of all parameters:

$$\rho = \begin{cases} 0.09\ in\ \ \Omega_1, \\ 2.5\ \ in\ \ \Omega_2, \\ 1.1\ \ in\ \ \Omega_3, \end{cases} \begin{cases} c_e\ =\ 1.5\Gamma_e, \\ c_i\ =\ 1.5\Gamma_i, \\ c_r\ =\ 0.007568, \end{cases} \Gamma_e = \begin{cases} 35\ \ in\ \ \Omega_1, \\ 40\ \ in\ \ \Omega_2, \\ 45\ \ in\ \ \Omega_3, \end{cases} \Gamma_i = \begin{cases} 35\ \ in\ \ \Omega_1, \\ 40\ \ in\ \ \Omega_2, \\ 70\ \ in\ \ \Omega_3, \end{cases}$$

$$\sigma = \begin{cases} 1.0\ \ in\ \ \Omega_1, \\ 2.4\ \ in\ \ \Omega_2, \\ 3.0\ \ in\ \ \Omega_3, \end{cases} A_e = \begin{cases} 200\ in\ \ \Omega_1, \\ 60\ \ in\ \ \Omega_2, \\ 81\ \ in\ \ \Omega_3, \end{cases} A_i = \begin{cases} 5\ \ \ \ \ \ \ in\ \ \Omega_1, \\ 0.00017\ \ in\ \ \Omega_2, \\ 0.02\ \ \ \ \ in\ \ \Omega_3, \end{cases}$$

$$A_r = \begin{cases} 1.8 \times 10^7/\rho\ \ \ in\ \ \Omega_1, \\ 9.0 \times 10^2/\rho^{1.5}\ \ in\ \ \Omega_2, \\ 2.1 \times 10^3/\rho^2\ \ \ in\ \ \Omega_3, \end{cases} A_{ei} = \begin{cases} 2000\ in\ \ \Omega_1, \\ 4000\ in\ \ \Omega_2, \\ 7000\ in\ \ \Omega_3, \end{cases} A_{er} = \begin{cases} 10\ \ in\ \ \Omega_1, \\ 140\ in\ \ \Omega_2, \\ 79\ \ in\ \ \Omega_3, \end{cases}$$

and $\mathcal{R}_1 = 90, \mathcal{R}_2 = 95, \mathcal{R} = 132$. In this paper, we use the energy conservation error defined in [15, 26] to evaluate the efficiency of different numerical methods for Eqs. (2.1a)-(2.1c). It is defined as follows:

$$Err = \left| \frac{\mathcal{E}_{enter}^n - (\mathcal{E}_{own}^n - \mathcal{E}_{own}^0)}{\mathcal{E}_{enter}^n} \right|,$$

https://doi.org/10.4208/nmtma.2016.m1523 Published online by Cambridge University Press

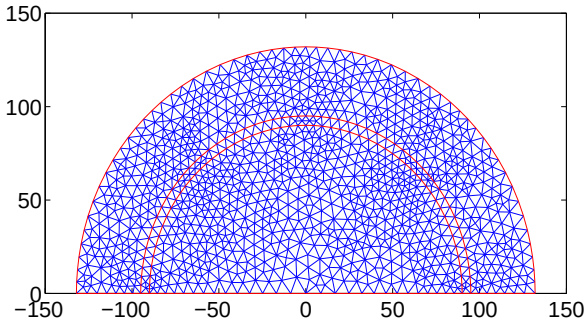


Figure 3: $Mesh0$.

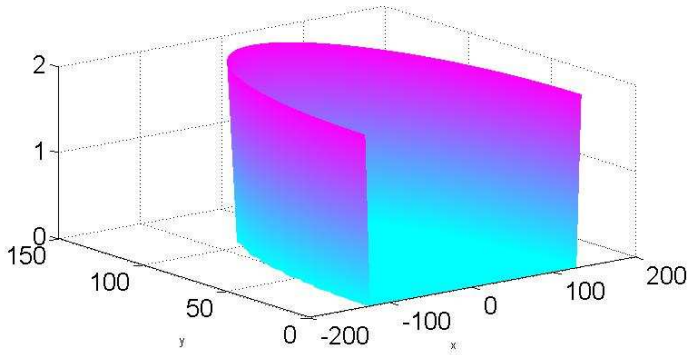


Figure 4: The stereogram of photon temperature at initial time.

where $\mathcal{E}^n_{enter}$ and $\mathcal{E}^n_{own}$ denote the total radiation energy importing from free boundary and the system energy at time t_n, respectively, and $\mathcal{E}^0_{own}$ the initial energy of the system at time $t_0 = 0$.

6.1. Results of Scheme I

In this part, we obtain the results of Scheme I. In the following computation, we use the unstructured triangular mesh with 2224 elements which is denoted by $Mesh0$. Fig. 3 and Fig. 4 depict the triangulation $Mesh0$ and the stereogram of photon temperature at initial time. There is no mixed material element, since the triangular mesh is fit with the interfaces between different subdomains. Here, we take a constant time step $\triangle t = 5 \times 10^{-4}$ and let the final state be $t = 14$.

Figs. 5-8 show the stereograms of photon temperature at time of 3, 6, 10, 14 in the numerical example. The first row of Table 1 shows the energy conservation error of Scheme I at six different physical time. It is worth mentioning that the numerical solutions are positive on the whole domain Ω throughout the process of computation.

https://doi.org/10.4208/nmtma.2016.m1523 Published online by Cambridge University Press

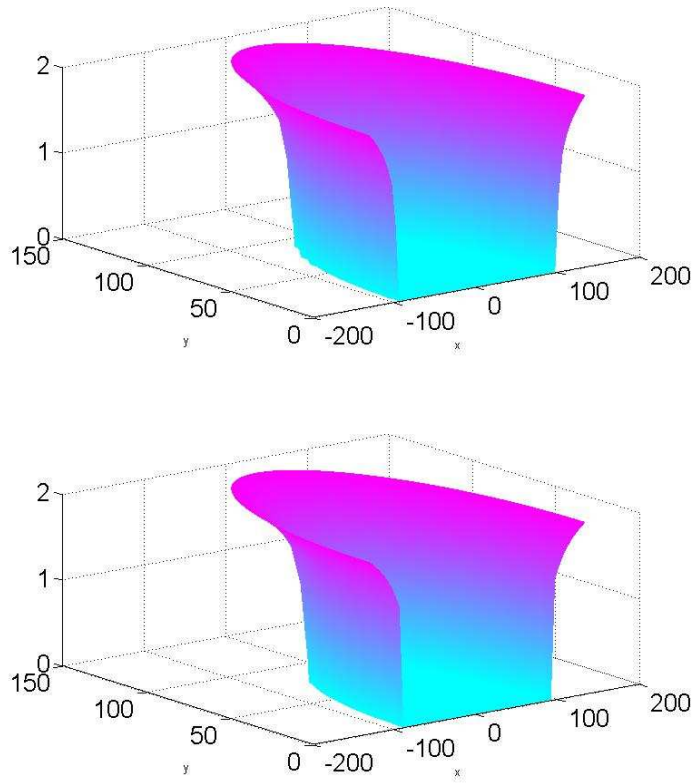


Figure 6: The stereogram of photon temperature at t=6 (Scheme I).

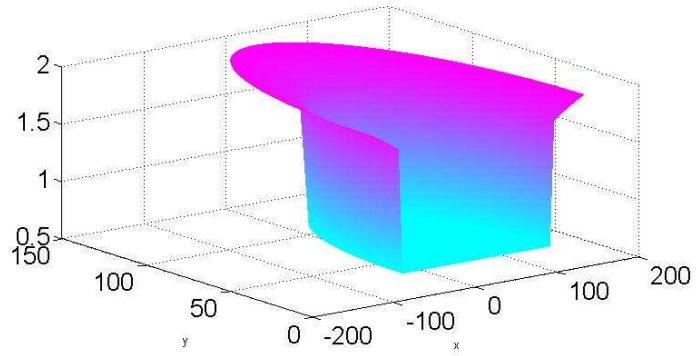


Figure 7: The stereogram of photon temperature at t=10 (Scheme I).

6.2. Results of Scheme II

In this part, the numerical results of Scheme II are presented. We still use the unstructured triangular mesh $Mesh0$, take a constant time step $\triangle t = 5 \times 10^{-4}$ and let

https://doi.org/10.4208/nmtma.2016.m1523 Published online by Cambridge University Press

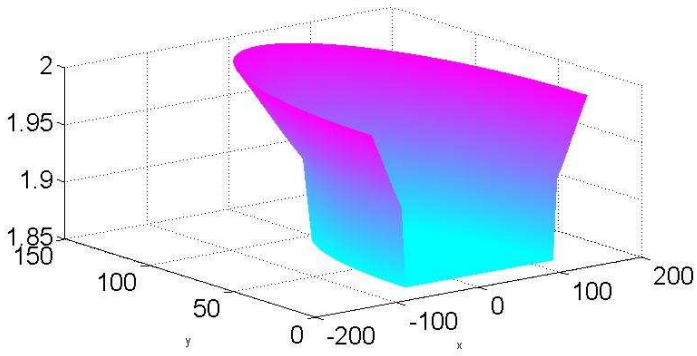


Figure 8: The stereogram of photon temperature at t=14 (Scheme I).

the final state be $t = 14$.

At the first time level, the numerical solutions appear negative values which lead to the breakdown of the computation. We use the post-processing techniques proposed in Section 4 to overcome this obstacle. The numerical results obtained by combining Scheme II with the global repair technique are denoted by Scheme II(G). The numerical results obtained by combining Scheme II with the cutoff method are denoted by Scheme II(C). Because the tendencies of Scheme I, Scheme II(G) and Scheme II(C) are similar, we just provide the stereograms of photon temperature at the final time in Fig. 9 and Fig. 10. The energy conservation errors of Scheme II(G) and Scheme II(C) are displayed in the second row and the third row of Table 1 respectively.

Table 1: Energy conservation error (%) of various numerical schemes.

Physical time	0.5	1.0	3.0	5.0	10.0	14.0
Scheme I	15.30	12.84	10.08	9.19	8.19	7.77
Scheme II(G)	18.38	14.93	11.24	10.09	8.98	8.46
Scheme II(C)	17.06	13.88	10.55	9.52	8.37	7.91
SFVES	15.39	12.90	10.12	9.22	8.22	7.81

6.3. Comparing with SFVES

In [15], a symmetric finite volume element scheme(SFVES) is proposed to solve 2-D 3-T radiation diffusion equations. In order to compare with SFVES, we use the same unstructured triangular mesh and time step size as mentioned above to proceed the numerical simulation. The same as Scheme I, the numerical solution arising from this SFVES is also positive in the whole process of computation. The stereogram of photon temperature at the final time is shown in Fig. 11. Comparing Figs. 8-11, there is no obvious differences between Scheme I and SFVES. In the forth row of Table 1, the energy conservation error of SFVES is displayed. From Table 1, it can be seen that

https://doi.org/10.4208/nmtma.2016.m1523 Published online by Cambridge University Press

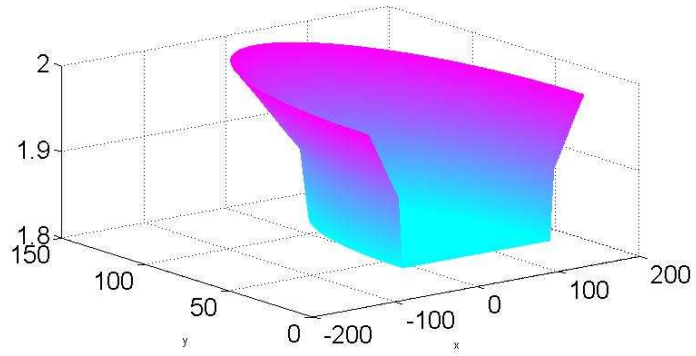
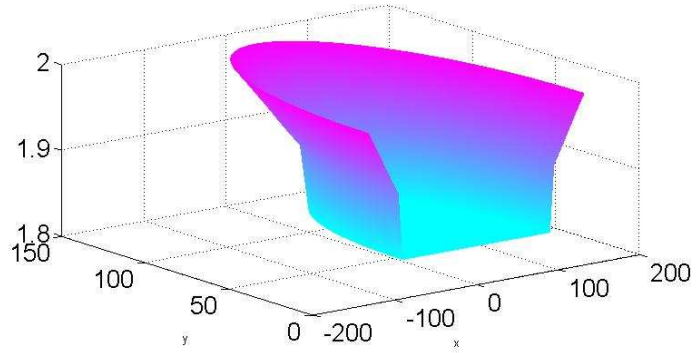


Figure 9: The stereogram of photon temperature at t=14 (Scheme II(G)).



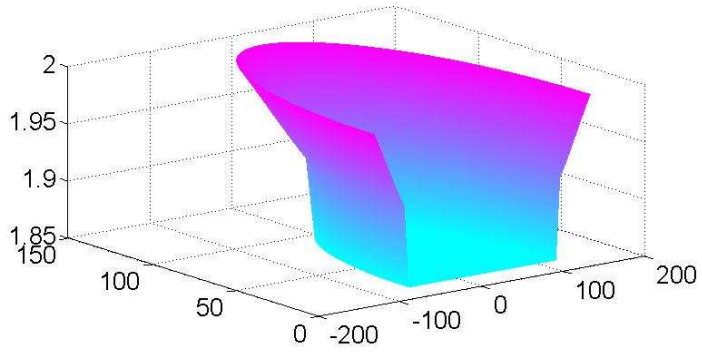
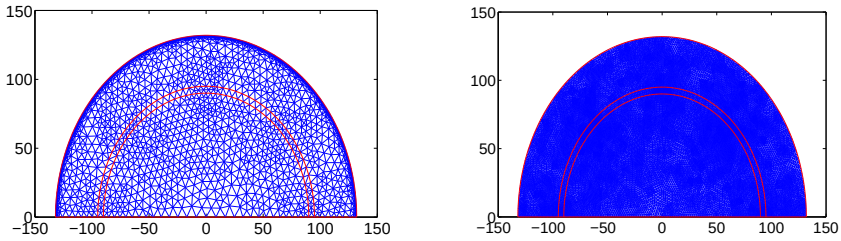


Figure 11: The stereogram of photon temperature at t=14 (SFVES).

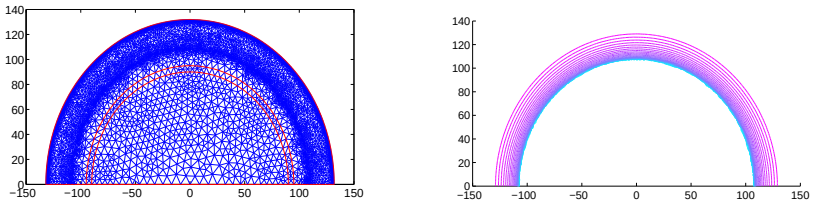
Scheme I is a little more effective in this respect of energy conservation.

https://doi.org/10.4208/nmtma.2016.m1523 Published online by Cambridge University Press



(a) (b)

Figure 12: Two triangulations of the computational domain Ω.



(a) Adaptive mesh (b) Contour of photon temperature

Figure 13: Adaptive mesh and contour of photon temperature at $t = 1$.

Table 2: Convergence accuracy of Scheme I.

Physical time	0.5	1.0	3.0	5.0	10.0	14.0
$Mesh0$	15.30	12.84	10.08	9.19	8.19	7.77
$CM1$	7.50	6.31	4.98	4.54	3.96	3.76
$CM2$	4.59	3.66	2.72	2.44	2.10	1.99

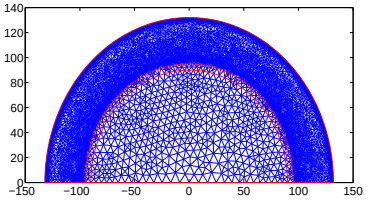
Table 3: Convergence accuracy of Scheme II(G).

Physical time	0.5	1.0	3.0	5.0	10.0	14.0
$Mesh0$	18.38	14.93	11.24	10.09	8.98	8.46
$CM1$	9.20	7.31	5.58	4.94	4.36	4.16
$CM2$	4.74	3.76	2.85	2.53	2.25	2.12

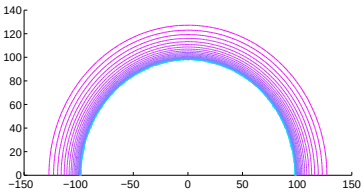
6.4. Numerical convergence on the energy conservation

Because the nonequilibrium radiation diffusion problem is relatively complex, it is extremely difficult to theoretically analyze the convergent accuracy of various numerical schemes. Therefore, we can only discuss the approximation accuracy from the view of numerical test. Let $CM1$ be a consistent refinement of $Mesh0$ and $CM2$ a consistent refinement of $CM1$. The numerical results obtained on $CM1$ and $CM2$ are presented in Table 2 and Table 3. From Table 2 and Table 3, we note that both Scheme I and Scheme II have first-order convergent accuracy.

https://doi.org/10.4208/nmtma.2016.m1523 Published online by Cambridge University Press

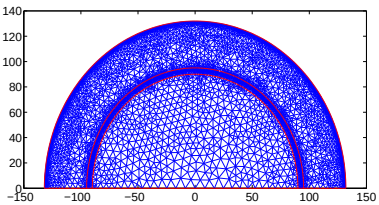


(a) Adaptive mesh

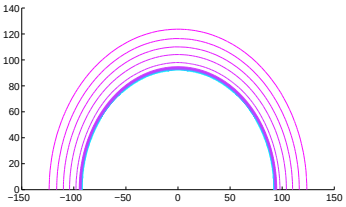


(b) Contour of photon temperature

Figure 14: Adaptive mesh and contour of photon temperature at $t = 3$.



(a) Adaptive mesh



(b) Contour of photon temperature

Figure 15: Adaptive mesh and contour of photon temperature at $t = 6$.

Table 4: Element average number and CPU time(h).

Items	$Mesh0$	$Mesh1$	Adaptive(G)	Adaptive(C)
Average num	2224	35584	10790	10337
CPU time	1.2	28.1	8.6	7.5

6.5. Results of mesh adaptation

In this part, we present the numerical results of mesh adaptation. From the former numerical results, we know that Scheme I is more better in terms of energy conservation and monotony. So Scheme I is employed to solve the PDEs (2.1a)-(2.1c) in the adaptive computation.

During the adaptive simulation, we split every triangular element marked for refinement into four by connecting the midpoints of three edges or into two by bisecting through the longest edge. If some element carries with hanging nodes on its edges, split the element into two by bisecting through the longest edge, until all the hanging nodes disappear. On the other hand, for the element ready to be coarsened, we firstly find out the elements coming from the same farther element with it, then merge all elements into one.

Because the adaptive meshes contain distorted elements, a part of numerical solution is negative. We still use the post-processing techniques to repair the numerical solution. We denote the examples combined with the global repair technique and cut-off method by Adaptive(G) and Adaptive(C) respectively. For comparison, we finish the numerical simulation with Scheme I on a dense mesh $Mesh1$ (Fig. 12(b)). The initial

https://doi.org/10.4208/nmtma.2016.m1523 Published online by Cambridge University Press

Table 5: Energy conservation error (%) of Adaptive(G), Adaptive(C).

Physical time	0.5	1.0	3.0	5.0	10.0	14.0
Adaptive(G)	3.64	2.77	1.99	1.82	1.73	1.64
Adaptive(C)	3.61	2.73	1.90	1.75	1.66	1.59
$Mesh1$	4.59	3.66	2.72	2.44	2.10	1.95

adaptive mesh is depicted in Fig. 12(a).

Figs. 13-15 show the contours of photon temperature and the adaptive meshes at time of 1, 3, 6 in the numerical example Adaptive(G). It can be seen that the adaptive meshes can capture the abrupt face of photon temperature and the regions on which elements mostly concentrate would change gradually as the abrupt face move towards the inner. Likewise, the same phenomena is also found in the numerical example Adaptive(C). Table 4 shows the average numbers of elements and CPU time. The energy conservation errors are filled in Table 5. We can see that the accuracy of the two adaptive simulations are both better than refining the mesh consistently, and the cost can be reduced by nearly two-thirds by using the adaptive algorithm.

7. Conclusion

This paper is concerned with two FVE schemes on triangular mesh for 2-D 3-T diffusion equations. Scheme I not only keep energy conservation well, but also preserve positivity of solutions for given meshes. Solutions of scheme II cannot preserve positivity, but the designed repair techniques are effective to overcome this disadvantage. From the numerical results, it can be seen that the mesh adaptation based on the posteriori error indicator can reduce the cost obviously without the loss of accuracy.

Acknowledgments This work was supported by Science Foundation of China Academy of Engineering Physics under Grant (number 11076014); National Natural Science Foundation of China under Grant (number 11371170).

References

[1] Berman A., Plemmons R. J.: Nonnegative matrices in the mathematical sciences. Academic Press, New York, 1979.
[2] Bi, C. J., Ginting, V.: A residual-type a posteriori error estimate of finite volume element method for a quasi-linear elliptic problem. Numerische Mathematik **114**(1), 107–132 (2009).
[3] Brenner, S. C., Scott, L. R.: The mathematical theory of finite element methods. Springer-Verlag, New York, 1994.
[4] Ciarlet, P. G.: The finite element method for elliptic problems (Studies in Mathematics and its Applications). North-Holland Publishing Co., Amsterdam, 4 (1978).

https://doi.org/10.4208/nmtma.2016.m1523 Published online by Cambridge University Press

[5] Cao, W. X., Zhang, Z. M., Zou, Q. S.: Is 2k-conjecture valid for finite volume methods? SIAM J. Numer. Anal. **53**, 942–962 (2015).
[6] Cao, W. X., Zhang, Z. M., Zou, Q. S.: Superconvergence of any order finite volume schemes for 1D general elliptic equations. J. Sci. Comput. **56**, 566–590 (2013).
[7] Chen, Z., Wu, J., Xu, Y.: High-order finite volume methods for elliptic boundary value problems. Adv. Comput. Math. **37**, 191–253 (2012).
[8] Chen, Z., Xu, Y., Zhang, Y.: Highter-order finite volume methods II: Inf-sup condition and uniform local ellipticity. J. Comput. and Applied. Math. **265**, 96–109 (2014).
[9] Chen, Z., Xu, Y., Zhang, Y.: A construction of highter-order finite volume methods. Math. Comp. **84**(292), 599–628 (2014).
[10] Eymard Robert, Gallouët Thierry, Hrebin Raphaèle: Finite volume methods (Handbook of Numerical Analysis). **7**, 713–1018 (2000).
[11] Furihata D.: Finite-dierence schemes for nonlinear wave equation that inherit energy conservation property. J. Comput. Appl. Math. **134**, 37–57 (2001).
[12] Fu, S. W., Huang, S. K., Li, Y. S.: Numerical simulation of indirectly driven high-convergence implosions. Chinese J. Comput. Phys. **16**, 162–166 (1999).
[13] Ham, F. E., Lien, F. S., Strong, A. B.: A fully conservative second-order finite difference scheme for incompressible flow on nonuniform grids. J. Comput. Phys. **177**, 117–133 (2002).
[14] Harte, J. A., Alley W. E., Bailey, D. S., Eddleman, J. L., Zimmerman, G. B.: Lasnex-a 2-d physics code for modeling icf. UCRL-LR-105821-96-4, 150–164 (1996).
[15] Jiang, J., Huang, Y. Q., Shu, S., Zeng, S.: Some new discretization and adaptation and multigrid methods for 2-D 3-T diffusion equations. J. Comput. Phys. **224**, 168–181 (2007).
[16] Langer, S. H., Scott, H. A., Marinak, M. M., Landen, O. L.: Comparisons of line emission from 2- and 3- dimension simulations of icf capsules to experiments. J. Quant. Spectrosc. Radiat. Transfer, 275–286 (2003).
[17] Le Potier, C.: Finite volume monotone scheme for highly anisotropic diffusion operators on unstructured triangular meshes. C. R. Acad. Sci. Paris, Ser. I **341**, 787–792 (2005).
[18] Lipnikov, K., Shashkov, M., Svyatskiy, D., Vassilevski, Yu.: Monotone finite volume schemes for diffusion equations on unstructured triangular and shape-regular polygonal meshes. J. Comput. Phys. **227**, 492–512 (2007).
[19] Liska, R., Shashkov, M.: Enforcing the discrete maximum principle for linear finite element solutions of second-order elliptic problems. Commun. Comput. Phys. **3**, 852–877 (2008).
[20] Li, R., Chen, Z., Wu, W.: The generalized difference methods for differential equations (Numerical analysis of finite volume methods). Marcel Dekker, New York, 2000.
[21] Li, R., Zhu, P.: Generalized difference methods for second order elliptic partial differential equations. I. The case of a triangular mesh. Numerical Mathematics. A Journal of Chinese Universities **4**, 360–375 (1982).
[22] Lin, Y. P., Yang, M., Zou, Q. S.: L-2 error estimates for a class of any order finite volume schemes over quadrilateral meshes. SIAM J. Numer. Anal. **53**, 2030–2050 (2015).
[23] Loubere, R. L., Staley, M., Wendroff, B.: The repair paradigm: New algorithms and applications to compressible flow. J. Comput. Phys. **211**, 385–404 (2006).
[24] Lu C. N., Huang, W. Z., Van Vleck, E. S.: The cutoff method for the numerical computation of nonnegative solutions of parabolic PDEs with application to anisotropic diffusion and lubrication-type equations. J. Comput. Phys. **242**, 24–36 (2013).
[25] Mikaelian, K. O.: LASNEX simulations of the classical and laser-driven RayleighC-Taylor

https://doi.org/10.4208/nmtma.2016.m1523 Published online by Cambridge University Press

instability. Phys. Rev. **42**, 4944–4951 (1990).
[26] Mo, Z. Y., Shen, L. J., Gabriel, W.: Parallel adaptive multigrid algorithm for 2-d 3-t diffusion equations. Int. J. Comput. Math. **81**, 361–374 (2004).
[27] Nie, C. Y., Shu, S.: A kind of symmetric finite volume scheme for the two-dimension three-temperature heat conduction equations. Natural Science Journal of Xiangtan University **26**, 18–22 (2004).
[28] Nie C. Y., Tan, M.: Some discussion on how to solve the two-dimension three-temperature heat conduction equations. Comm. On Appl. Math. And Comput. **22**(1), 57–61 (2008).
[29] Ober, C. C., Shadid, J. N.: Studies on the accuracy of time-integration methods for the radiation-diffusion equations. J. Comput. Phys. **195**, 743–772 (2004).
[30] Perot B.: Conservation properties of unstructured staggered mesh Schemes. J. Comput. Phys. **159**, 58–89 (2002).
[31] Shashkov, M., Wendroff, B.: The repair paradigm and application to conservation laws. J. Comput. Phys. **198**, 265–277 (2004).
[32] Sheng, Z. Q., Yuan, G. W.: A nine point scheme for the approximation of diffusion operators on distorted quadrilateral meshes. SIAM J. Sci. Comput. **30**, 1341–1361 (2008).
[33] Stals, L.: Comparison of non-linear solvers for the solution of radiation transport equations. Electronic Transactions on Numerical Analysis **15**, 78–93 (2003).
[34] Sheng, Z. Q., Yue, J. Y., Yuan, G. W.: Monotone finite volume schemes of nonequilibrium radiation diffusion equations on distorted meshes. SIAM J. Sci. Comput. **31**, 2915–2934 (2009).
[35] Varga R.: On a discrete maximum principle. SIAM J. Numer. Anal. **3**, 355–359 (1966).
[36] Wang, S., Yuan, G. W., Li, Y. H., Sheng, Z. Q.: Discrete maximum principle based on repair technique for diamond type scheme of diffusion problems. Int. J. Numer. Meth. Fluids **70**, 1188–1205 (2012).
[37] Wu H. J., Li, Y. H., Li, R. H.: Adaptive generalized difference finite volume computations for two dimensional nonlinear parabolic equation. Chinese J. Comput. Phys. **20**, 298–306 (2003).
[38] Xu, X. W., Mo, Z. Y., An, H. B.: Algebraic two-level iterative method for 2-D 3-T radiation diffusion equations. Chinese J. Comput. Phys. **26**, 1–8 (2009).
[39] Xu, J., Zikatanov, L.: A monotone finite element scheme for convection diffusion equations. Math. Comp. **68**, 1429–1446 (1999).
[40] Xu, J. C., Zou, Q. S.: Analysis of linear and qualratic simplicial finite volume methods for elliptic equations. Numerische Mathematik **111**, 469–492 (2009).
[41] Xu, J. C., Zhang, Z. M.: Analysis of recovery type a positeriori error estimators for mildly structured grids. Mathematics of Computation **73**(247), 1139–1152 (2004).
[42] Yang, X. B., Huang, W. Z., Qiu, J. X.: A moving mesh finite difference method for equilibrium radiation diffusion equations. J. Comput. Phys. **298**, 661–677 (2015).
[43] Zhao, Q., Yuan, G. W.: Analysis and construction of cell-centered finite volume scheme for diffusion equations on distorted meshes. Comput. Meth. Appl. Mech. Engrg. **198**, 3039–3050 (2009).
[44] Zhao, X. K., Chen, Y. L., Gao, Y. N., Yu, C. H., Li, Y. H.: Finite volume element methods for nonequilibrium radiation diffusion equations. Int. J. Numer. Meth. Fluids **73**, 1059–1080 (2013).
[45] Zou, Q. S., Veeser, A., Kornhuber, R., Graser, C.: Hierarchical error estimates for the energy functional in obstacle problems. Numerische Methematik **117**(4), 653–677 (2001).
[46] Zou, Q. S.: Hierarchical error estimates for finite volume approximation solution of elliptic equations. Applied Numerical Mathematics **60**, 142–153 (2010).

https://doi.org/10.4208/nmtma.2016.m1523 Published online by Cambridge University Press

[47] Zou, Q. S., Kornhuber, R.: Efficient and reliable hierarchical error estimates for the discretization error of elliptic obstacle problems. Math. Comp. **80**, 69–88 (2011).
[48] Zhang, Z. M., Yan, N. N.: Recovery type a posteriori error estimates in finite element methods. Korean J. Comput. & Appl. Math. **8**(2), 235–251 (2001).
[49] Zhang, Z. M., Zou, Q. S.: A family of finite volume schemes of arbitrary order on rectangular meshes. J. Sci. Comput. **58**, 308–330 (2014).
[50] Zhang, Z. M., Zou, Q. S.: Vertex-centered finite volume schemes of any order over quadrilateral meshes for elliptic boundary value problems. Numer. Math. **130**, 363–393 (2015).

https://doi.org/10.4208/nmtma.2016.m1523 Published online by Cambridge University Press